

3-DoF Magnetically Actuated Robotic Manipulator for Precision Soft Tissue Resection

Majid Roshanfar^{1,*}, Changyan He^{2,*}, Long Huang³, Zhaoxin Li⁴, Lingbo Cheng², Dale J. Podolsky^{1,5}, Thomas Looi¹, and Eric Diller^{4,6}

Abstract—Magnetically actuated small-scale robotic end-effectors offer a promising alternative to conventional cable-driven systems for dexterous surgical applications by eliminating mechanical power transmission, reducing friction, and enabling significant miniaturization. However, many existing systems remain constrained to 1- or 2-degree-of-freedom (DoF) movements, which, while suitable for basic manipulation, still fall short in providing the dexterity required for more complex surgical procedures. This paper introduces a novel design for a 3-DoF magnetic robotic manipulator for soft tissue resection in brain surgery. The proposed system incorporates three orthogonal articulated joints, all actuated by a single onboard magnet, enabling full rotational motion (pitch, yaw, roll) while maintaining a compact and lightweight form factor. Two specialized end-effectors—a 3-DoF rotary cutter and a 3-DoF swing cutter—were developed to demonstrate the versatility of the proposed design in executing precise tissue resection tasks. A kinematic model was formulated to achieve independent actuation of each joint, ensuring dynamic stability through compensation for gravitational and inertial forces. Experimental results demonstrated that the manipulators successfully achieved: (1) 3-DoF motion within a workspace of $[360^\circ; -87^\circ \text{ to } 87^\circ; -83^\circ \text{ to } 83^\circ]$ for the swing cutter and $[360^\circ; -78^\circ \text{ to } 78^\circ; \text{continuous rotation}]$ for the rotary cutter; (2) maximum push forces of 20 mN for the swing cutter and 70 mN for the rotary cutter under a magnetic field of just 10 mT; and (3) effective cutting performance in 1% concentration agar gel phantoms. These findings highlight the promise of 3-DoF magnetic robotic manipulators in advancing minimally invasive surgical interventions.

I. INTRODUCTION

Magnetic actuation represents a paradigm shift in small-scale medical device development, enabling precise remote

This work was supported by Canadian Institutes of Health Research (CIHR) Grant 452287, the University of Newcastle Startup Support, and the National Natural Science Foundation of China.

* The authors contributed equally to this work.

¹M. Roshanfar, D.J. Podolsky, and T. Looi are with The Wilfred and Joyce Posluns Centre for Image Guided Innovation & Therapeutic Intervention (PCIGITI) at the Hospital for Sick Children (SickKids), Toronto, Ontario, Canada. majid.roshanfar@sickkids.ca; thomas.looi@sickkids.ca

²C. He and L. Cheng are with the School of Engineering, University of Newcastle, NSW, Australia. changyan.He@newcastle.edu.au

³L. Huang is with the College of Mechanical Engineering, Changsha University of Science and Technology, China.

⁴Z. Li and E. Diller are with the Department of Mechanical and Industrial Engineering, University of Toronto, Toronto, Ontario, Canada.

⁵D.J. Podolsky is also with the Division of Plastic & Reconstructive Surgery, The Hospital for Sick Children (SickKids), Toronto, Ontario, Canada. dale.podolsky@sickkids.ca

⁶E. Diller is also with the Robotics Institute, and the Department of Biomedical Engineering at the University of Toronto, Toronto, Ontario, Canada. ediller@mie.utoronto.ca

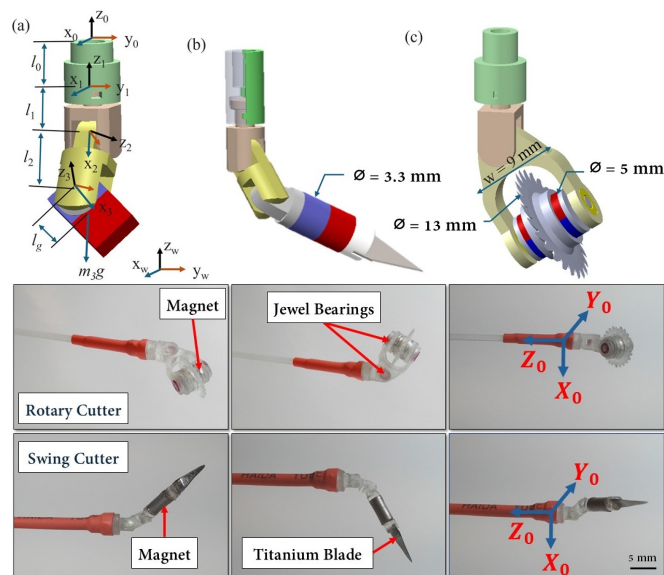


Fig. 1: Proposed 3-DoF magnetic robotic manipulator. Top: (a) Schematic design showing coordinate frames with three orthogonal rotational joints. Coordinate frames are set at the joint centers, in which z -axis aligns with the rotational axis and x -axis points to its adjacent joint. (b) Implementation as a swing cutter ($\varnothing_{magnet} = 3.3 \text{ mm}$). (c) Implementation as a rotary cutter with a circular saw blade ($\varnothing_{magnet} = 5 \text{ mm}$, $\varnothing_{blade} = 13 \text{ mm}$). Bottom: Prototype configurations demonstrating the manipulator's versatility. The top row shows the rotary cutter with an embedded magnet enabling multiple cutting orientations. The bottom row displays the swing cutter with a titanium blade attached to the magnetic, showcasing various cutting angles achievable through remote magnetic actuation.

manipulation without the constraints of onboard power supplies or complex mechanical transmissions. By harnessing external magnetic field-generated forces and torques, these devices achieve wireless control, dramatically simplifying design requirements while enhancing miniaturization potential [1]. Magnetic fields, typically generated using permanent magnets or electromagnetic coils, offer scalability and adaptability across diverse biomedical applications. Tethered magnetic catheters and guidewires have demonstrated clinical utility in procedures ranging from stent placement [2] and vascular ablation [3], [4] to blood clot clearance [5] and minimally invasive surgeries (MIS) [6], showcasing their precision and versatility [7]. However, these applications predominantly involve simple, decoupled, or single-directional

movements with straightforward control strategies. More sophisticated surgical maneuvers, such as tissue cutting, grasping, or suturing, demand end-effectors with enhanced dexterity and multiple degrees of freedom (DoFs), presenting considerable challenges for magnetic actuation systems.

Recent innovations have explored magnetic robotic systems for complex tissue operations with promising results. Notable developments include wristed grippers for tissue manipulation [8], twisted-string-actuated forceps for resection [9], tetherless scissors for tissue cutting [10], and flexible joint-based grippers for handling soft tissues [11]. There has also been research addressing the challenge of utilizing two magnetically actuated instruments, which is essential for enabling bimanual operations [12]. These breakthroughs demonstrate the viability of magnetic actuation for intricate surgical tasks while preserving compact, minimally invasive profiles. When compared to conventional cable/tendon-driven mechanisms, magnetic robotic tools offer distinct advantages such as reduced friction, modular design principles, and superior miniaturization potential. These characteristics make them particularly well-suited for integration into endoscopic platforms for MIS interventions.

Despite these advances, current magnetic tools remain constrained by their limited DoF, typically no more than two, which significantly restricts their dexterity in performing complex surgical maneuvers. Furthermore, many existing designs incorporate multiple small onboard magnets, introducing system instability through inter-magnet attractions or repulsions. Traditional robotic end-effectors, exemplified by the da Vinci surgical system, achieve superior six-DoF dexterity through stacked, cable-driven joints [13], but this approach inevitably increases system complexity, friction forces, and mechanical wear. Alternative strategies have emerged, such as integrating magnetic end-effectors with flexible robotic positioners like concentric tube robots [14], [15]. While this approach adds supplementary DoFs to magnetic tools, it simultaneously increases the system's overall complexity and physical footprint, complicating deployment in already crowded operating environments.

This work addresses these fundamental limitations by introducing a novel 3-DoF magnetic robotic manipulator featuring three orthogonal rotational joints actuated by a single onboard magnet (Fig. 1). This innovative design enables complete directional adjustments, including pitch, roll, and yaw motions, while eliminating the instability issues associated with multiple-magnet configurations. Additionally, the compact arrangement significantly enhances miniaturization potential, making the manipulator exceptionally suitable for MIS applications. We further develop a comprehensive model that ensures dynamic stability by accurately compensating for gravitational and inertial forces throughout the operation. To demonstrate the versatility and clinical utility of our proposed manipulator, we develop two specialized end-effectors: a swing cutter and a rotary cutter. The swing cutter mimics a surgeon's wrist holding a scalpel, providing dexterous rotational movements in three directions for precise incisions. The rotary cutter, a first-of-its-kind

miniature spinning tool, delivers continuous tissue-cutting capability with adjustable cutting planes in two directions. Both tools are specifically designed for tissue resection tasks and undergo rigorous experimental evaluation for motion performance and cutting effectiveness.

A critical consideration in magnetic actuation systems is the significant reduction of magnetic field strength with distance, raising questions about whether sufficient force can be transmitted to magnetic tools for demanding surgical tasks such as tissue cutting. Previous research, including [16], demonstrates that moderate magnetic field strengths (approximately 30 mT) can generate forces on the order of 0.1 N, sufficient for manipulating soft brain tissue [17]. Building on this foundation, our work focuses specifically on brain tissue resection, an essential component of neurosurgical procedures including corpus callosotomy and tumor removal. Corpus callosotomy involves severing the nerve fiber band connecting the brain hemispheres to treat epilepsy, while tumor removal requires meticulous excision of diseased tissue for brain cancer treatment. To assess cutting performance, we fabricated a phantom using agar gel, a commonly used material that closely mimics the mechanical properties of brain tissue [18]. Both cutting mechanisms undergo systematic testing on this agar gel phantom to assess their cutting efficacy. Accordingly, the primary contributions of this paper are:

- Development of a compact 3-DoF magnetic robotic manipulator with three orthogonal joints actuated by a single onboard magnet, enabling precise pitch, yaw, and roll control.
- Formulation of a kinematic model for independent and dynamically stable actuation of all joints.
- Design and implementation of two dexterous magnetic end-effectors: a swing cutter and a rotary cutter, each tailored for precision soft tissue resection.
- Experimental validation of the system's motion capabilities and cutting performance in phantoms, demonstrating its potential for neurosurgical applications.

II. DESIGN OF THE 3-DOF MAGNETIC END-EFFECTOR

This section presents the design of our magnetic end-effector aimed at replicating human wrist capabilities for dexterous manipulations, including pitch, yaw, and roll motions. The design incorporates three key innovations: orthogonal joint arrangement, single-magnet actuation, and decoupled motion control.

A. Design Principles and Magnetic Actuation

Our design utilizes three rotational joints arranged orthogonally to provide articulation in three independent directions. Unlike existing magnetic robotic end-effectors that require multiple embedded magnets, our approach implements a single onboard magnet positioned at the robot's tip, as illustrated in Fig. 2. This design choice significantly reduces system complexity while maintaining full directional control. The principles of magnetic actuation that govern our system are well-established in literature [19]. When subjected to an

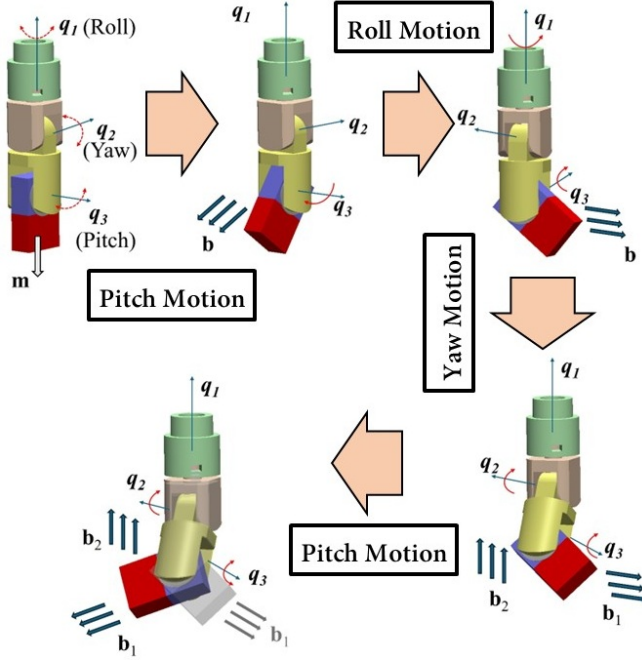


Fig. 2: The 3-DoF magnetic end-effector's motion capabilities: Sequential illustration of the yaw-roll-pitch motion sequence. The magnetic vectors (\mathbf{b} , \mathbf{b}_1 , \mathbf{b}_2) indicate the direction of the applied magnetic field for each motion state.

external magnetic field $\mathbf{b} = [b_x, b_y, b_z]$, a magnetic object experiences a field torque $\boldsymbol{\tau} = [\tau_x, \tau_y, \tau_z]$ that rotates the magnet to align its magnetization $\mathbf{m} = [m_x, m_y, m_z]$ with the field direction, as expressed in (1). Although magnetic force can also be generated, it becomes negligible when the external field is near-uniform, and is therefore not considered.

$$\boldsymbol{\tau}_b = \mathbf{m} \times \mathbf{b} \quad (1)$$

B. Joint Configuration and Motion Control

The three joints are designated as q_1 , q_2 , and q_3 , corresponding to roll, yaw, and pitch motions, respectively (Fig. 2). We conceptualize the roll and yaw motions as posture adjustment processes, while the pitch motion serves as the cutting execution process. For posture adjustment, the yaw motion (q_2) is actuated by applying a magnetic field in the q_1q_3 plane, causing the magnet to tilt accordingly. When roll motion (q_1) is required, the system first establishes a slight tilting angle through a pitch motion. The field direction is then rotated around the q_1 axis to adjust the magnet's orientation, completing the roll. Upon completion of the yaw motion, the tilting angle can be maintained while initiating a pitch motion by adjusting the field direction within the tilting plane. The pitch motion (q_3) is initiated by applying a field in the plane orthogonal to the q_3 axis, with the in-plane direction of the field changing to guide the magnet's heading. This configuration allows for precise rotational control across all three DoF, as illustrated in Fig. 2.

III. KINEMATIC MODELING

We first build a common kinetic-static model for the 3-DoF end-effector, and then apply it to the two specific tools.

As shown in Fig. 1, we set coordinate frames at the rotational center of each joint as $\{1\}, \{2\}, \{3\}$, and the base frame at the tool anterior end as $\{0\}$. The world frame is denoted as $\{w\}$. As a common practice, the z -axis is set along the joint motion direction. The kinematics transformation of the robot can be represented by a homogeneous matrix:

$${}^i_w\mathbf{T} = \begin{bmatrix} {}^i_w\mathbf{R} & {}^i_w\mathbf{p} \\ \mathbf{0} & 1 \end{bmatrix} \quad (2)$$

The rotation matrix ${}^i_w\mathbf{R}$ can be expressed as:

$${}^i_w\mathbf{R} = [\mathbf{n}_i, \mathbf{o}_i, \mathbf{a}_i] \quad (3)$$

where \mathbf{n}_i , \mathbf{o}_i , and \mathbf{a}_i represent the x-axis, y-axis, and z-axis of the i -th coordinate frame, respectively. The equilibrium equation for joint 3 can be established as:

$$(l_g \mathbf{n}_3 \times \mathbf{f}_{g3})^\top \mathbf{a}_3 + J_3 \ddot{q}_3 + \tau_{f3} + \tau_{\text{tissue}} = (|\mathbf{m}| \mathbf{n}_3 \times \mathbf{b})^\top \mathbf{a}_3 \quad (4)$$

where l_g is the length from the magnet center to the \mathbf{z}_3 -axis, which equals zero for the rotary cutter because its magnet's center line is colinear with the robot's \mathbf{z}_3 -axis. J_3 is the moment of inertia relative to \mathbf{z}_3 -axis, \ddot{q}_3 is the angular acceleration, τ_{f3} is the resistance torque caused by the joint friction, which is estimated experimentally. τ_{tissue} is the tool-to-tissue interaction force, which could be obtained through the experiments. $\mathbf{f}_{g3} = [0, 0, -m_3g]^\top$ is the force caused by the gravity in which m_3 represents the mass of the magnet, $|\mathbf{m}|$ is the magnitude of the magnet dipole moment. Similarly, the equilibrium equation can be resolved for joint 2 by removing the interaction force, as below:

$$((l_g \mathbf{n}_3 + l_2 \mathbf{n}_2) \times \mathbf{f}_{g3})^\top \mathbf{a}_2 + J_2 \ddot{q}_2 + \tau_{f2} = (|\mathbf{m}| \mathbf{n}_3 \times \mathbf{b})^\top \mathbf{a}_2 \quad (5)$$

where l_2 is the length between \mathbf{z}_3 -axis and \mathbf{z}_2 -axis, J_2 , \ddot{q}_2 , and τ_{f2} are the moment of inertia, angular acceleration, and frictional torque for joint 2. Lastly, the equilibrium equation can be obtained for joint 1 as:

$$J_1 \ddot{q}_1 + \tau_{f1} = (|\mathbf{m}| \mathbf{n}_3 \times \mathbf{b})^\top \mathbf{a}_1 \quad (6)$$

where J_1 , \ddot{q}_1 , and τ_{f1} are the moment of inertia, angular acceleration, and frictional torque for joint 1. With the above-described three equilibrium equations, the actuating field \mathbf{b} can be derived by giving the input of desired joint angles $q_{id}, i = 1, 2, 3$. To ensure the motion smoothness, we use the cubic polynomial interpolation to calculate the joint angle $q_i(t)$ when the desired angle q_{id} is given, as below:

$$q_i(t) = q_{i0} + \frac{3}{\delta t^2} (q_{id} - q_{i0}) t^2 - \frac{2}{\delta t^3} (q_{id} - q_{i0}) t^3 \quad (7)$$

where q_{i0} is the initial angle for the joint i , $i = 1, 2$ and δt is the transition time that the expected motion takes. The joint-3's motion trajectories of the two tools are different because of their distinct motion patterns and therefore need to be designed separately. The swing cutter has a reciprocating motion at its joint 3. When the movement starts, the joint moves from its center position q_{30}^s to its maximum angle $q_{30}^s + A$ within a transition time δt , and then reciprocates between

the extreme positions $[q_{30}^s - A, q_{30}^s + A]$. The superscription s represents the swing cutter and A is the reciprocation amplitude. This process can be formulated as:

$$q_3^s(t) = \begin{cases} q_{30}^s + \frac{3}{\delta t^2}A(t-t_0)^2 - \frac{2}{\delta t^3}A(t-t_0)^3 & t \leq t_0 + \delta t \\ A\cos(\omega(t-\delta t-t_0)) + q_{30}^s & t > t_0 + \delta t \end{cases} \quad (8)$$

where ω represents the angular frequency of the swing cutter and t_0 is the timing at which the motion starts. The rotary cutter has a continuous rotation motion at its joint 3. When the movement starts, joint 3 accelerates from stationary to an angular velocity ω within a transition time δt , then keeps rotating at the velocity of ω . This can be described as:

$$q_3^r(t) = \begin{cases} q_{30}^r + \frac{\omega}{2\delta t}(t-t_0)^2 & t \leq t_0 + \delta t \\ q_{30}^r + \frac{1}{2}\omega\delta t + \omega(t-\delta t-t_0) & t > t_0 + \delta t \end{cases} \quad (9)$$

where the superscription r represents for the rotary cutter. When desired motions are given for the three joints, the required actuating field \mathbf{b} can be resolved by substituting the motion trajectories in (7), (8), and (9) to the equilibrium equations (4), (5), and (6). In the implementation, the following rules need to be obeyed to avoid null commands: (a) The movements of the three joints need to be actuated in sequence, i.e., when one joint moves, the other two need to be kept unchanged. (b) The movement of joint 1 depends on a non-zero angle of joint 2 or 3. The final form of the magnetic field component is calculated as follows:

$$\begin{aligned} B_x &= -\frac{f_3s_2X_1 - f_2s_3X_1 + f_2h_3X_2 - f_3h_2X_2 + h_2s_3X_3 - h_3s_2X_3}{m(f_3h_2s_1 - f_2h_3s_1 - f_3h_1s_2 + f_1h_3s_2 + f_2h_1s_3 - f_1h_2s_3)} \\ B_y &= -\frac{f_1s_3X_1 - f_3s_1X_1 + f_3h_1X_2 - f_1h_3X_2 + h_3s_1X_3 - h_1s_3X_3}{m(f_3h_2s_1 - f_2h_3s_1 - f_3h_1s_2 + f_1h_3s_2 + f_2h_1s_3 - f_1h_2s_3)} \\ B_z &= -\frac{f_2s_1X_1 - f_1s_2X_1 + f_1h_2X_2 - f_2h_1X_2 + h_1s_2X_3 - h_2s_1X_3}{m(f_3h_2s_1 - f_2h_3s_1 - f_3h_1s_2 + f_1h_3s_2 + f_2h_1s_3 - f_1h_2s_3)} \end{aligned} \quad (10)$$

A. Implementation for the Swing and Rotary Cutters

Based on the above theoretical framework, we implement a three-phase control strategy for both the swing cutter and rotary cutter as illustrated in Fig. 3. The control phases are structured identically for both tools:

- **Phase 1 (0-1s):** Joint 2 (yaw) is adjusted from 0° to 20° using cubic polynomial trajectory, while joints 1 and 3 remain at their initial positions (0°).
- **Phase 2 (1-2s):** Joint 1 (roll) is adjusted from 0° to 30° using cubic polynomial trajectory, while joint 2 is maintained at 20° and joint 3 remains at 0° .
- **Phase 3 (2-7s):** Joints 1 and 2 are maintained at their final positions (30° and 20° respectively), while joint 3 executes the tool-specific cutting motion.

For the swing cutter in Phase 3, joint 3 first transitions from 0° to its maximum amplitude of 45° within 1-second using equation (8), then oscillates between -45° and $+45^\circ$ with a period of 2.5 seconds, completing approximately two full oscillation cycles over 5 seconds. For the rotary cutter in Phase 3, joint 3 accelerates from 0° to a constant angular velocity of 4π rad/s (2 revolutions per second) within 1

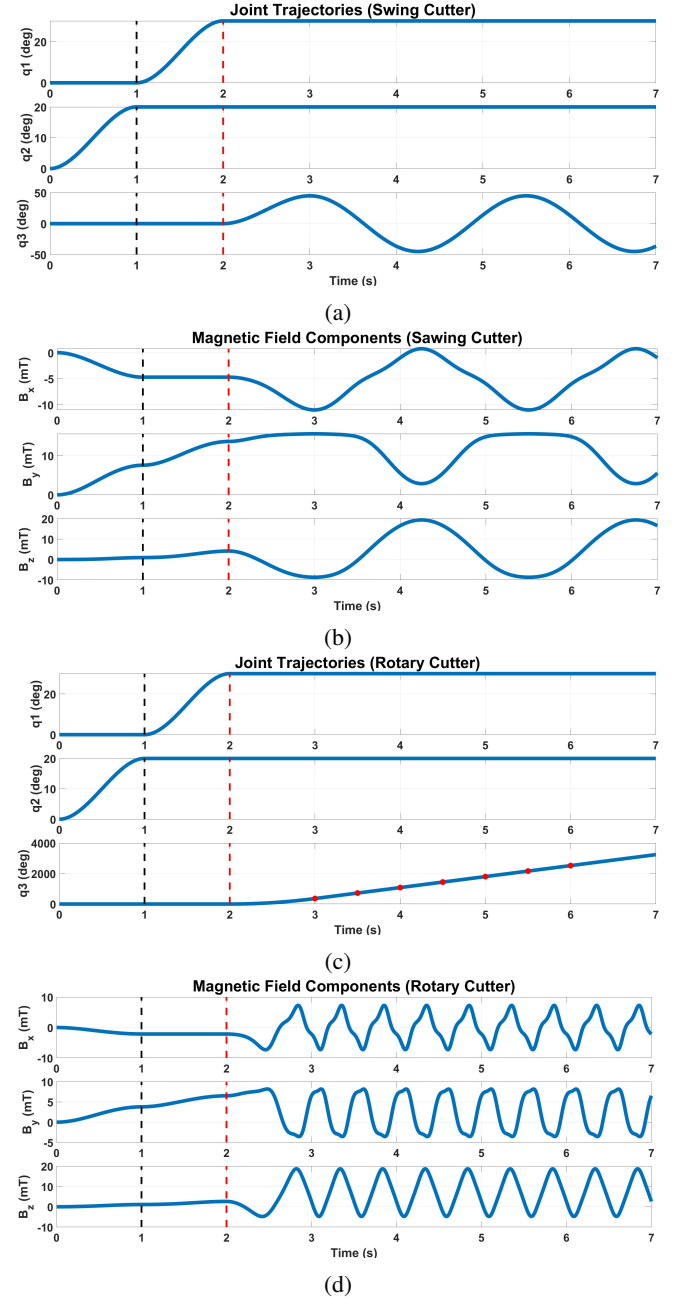


Fig. 3: Three-phase strategy for the swing cutter (a,b) and rotary cutter (c,d). Phase 1 (0-1s): Joint 2 adjustment. Phase 2 (1-2s): Joint 1 adjustment. Phase 3 (2-7s): Joint 3 cutting motion. In (c), red dots indicate each complete rotation.

second using equation (9), then continues rotating at this constant velocity, completing approximately 8 full rotations over 5 seconds as indicated by the markers in Fig. 3(d). To enhance stability during lifting operations, the coordinate system is rotated so that the lifting direction aligns with the x -axis. This rotation is achieved by the transformation matrix, which maps the original x -axis to the new z -axis, preserves the y -axis, and maps the original z -axis to the new x -axis. This coordinate rotation ensures that the gravity compensation is primarily contributed by the B_x component of the magnetic field. Fig. 3(b) shows the resulting mag-

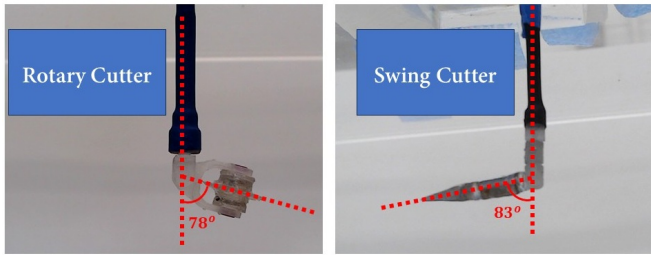


Fig. 4: Motion range evaluation for rotary and swing cutters.

netic field components over time for the swing cutter. The magnetic field components for the rotary cutter, shown in Fig. 3(d), exhibit different patterns due to the continuous rotation of joint 3. The B_x component shows oscillatory behavior between -8 mT and +8 mT but with a higher frequency corresponding to the continuous rotation. The B_y and B_z components also show higher frequency oscillations. Both cutters demonstrate smooth transitions between phases in their magnetic field components, ensuring continuous and stable actuation throughout the entire motion sequence. The primary difference between the two cutters lies in the nature of their joint 3 motion, which is the swing cutter performs reciprocating oscillations suitable for sawing actions, while the rotary cutter performs continuous rotation.

IV. EXPERIMENTS AND RESULTS

A. Tools Fabrication

We prototyped the parts of two tools using a 3D printer (Formlabs) with both Tough Resin and Clear V4 resin materials. Jewel bearings (Swiss Jewel, R158) were used in the pin joints to reduce friction where necessary. It is worth noting that friction in the second joint can help maintain the joint in a stationary position during posture adjustments. However, introducing friction in the tip joint would hinder the smooth rotation of the blade in the rotary cutter. This trade-off highlights the importance of balancing joint friction for mechanical stability versus motion efficiency. The blade of the swing cutter was manually filed from a 1 mm thick titanium sheet, while the blade of the rotary cutter was 3D-printed due to its more complex shape. The swing cutter has a cylindrical shape with dimensions of $\varnothing 3 \text{ mm} \times 5 \text{ mm}$, and the rotary cutter features a circular blade with a diameter of 5 mm and a slim neck measuring $\varnothing 3 \text{ mm} \times 3 \text{ mm}$.

B. Joint Motion Range Evaluation

The range of motion of the two tools was evaluated using the experimental setup illustrated in Fig. 4. An external magnetic field was generated using a previously developed electromagnetic navigation system (ENS) [20]. Each tool was actuated to sequentially drive its joints to their mechanical limits. At each extreme position, images were captured to document the maximum range of joint articulation. The recorded images were post-processed to extract the corresponding joint angles. The measured angular ranges for each joint are summarized in Table I. The estimated reachable workspace forms a spherical segment, sufficient for local manipulation tasks in confined surgical environments.

TABLE I: Measured range of motion for each joint.

Tool	Joint	Angular Range ($^\circ$)
Swing Cutter	Joint 1	0 to 360
	Joint 2	-87 to 87
	Joint 3	-83 to 83
Rotary Cutter	Joint 1	0 to 360
	Joint 2	-78 to 78
	Joint 3	$-\infty$ to ∞

TABLE II: Cutting performance evaluation on agar gel (1%).

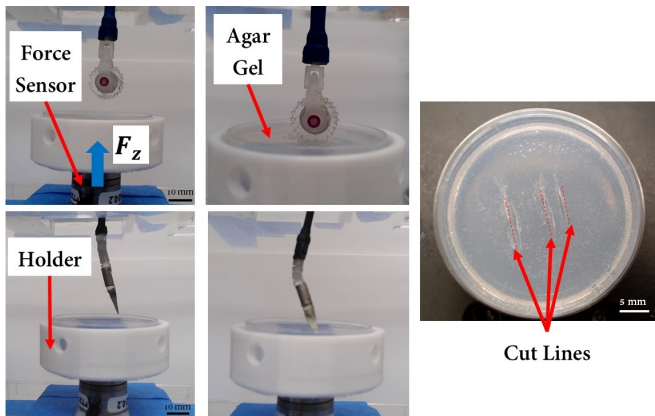
Tool	Average Cutting Length (mm)	Maximum Cutting Force (N)
Swing Cutter	8.8	0.02
Rotary Cutter	11.4	0.07

C. Cutting performance evaluation

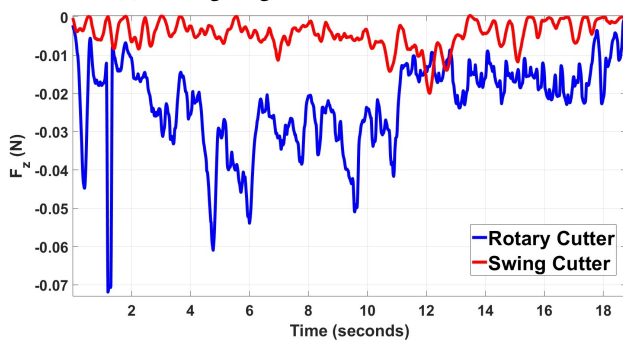
The cutting tools were evaluated using an agar gel phantom, which was mounted on an ATI Nano17 6-DoF force/torque sensor (see Fig. 5(a)). This sensor is made from titanium, ensuring that the force measurements are not influenced by external magnetic fields. The preparation of the agar gel phantom involved manually mixing agarose powder with distilled water at room temperature, followed by heating the mixture in a microwave for approximately 30 seconds until fully dissolved. The heated solution was then poured into a custom-designed 3D-printed mold and allowed to cool and solidify. Agarose gel is widely used in biomedical experiments as a tissue-mimicking material due to its mechanical properties being similar to those of brain tissue. During testing, each magnetic cutter was positioned vertically in contact with the surface of the agarose phantom. A rotating magnetic field of 10 mT was applied to actuate the cutter and initiate the cutting motion. Following this, the cutter tip was manually advanced further to complete the full cutting trajectory through the gel. After each cutting attempt, the resulting cutting length and corresponding force measurements were recorded. A summary of the measured values is provided in Table II and Fig. 5(b). The swing cutter demonstrated superior cutting performance, achieving longer cutting lengths with lower applied forces compared to the rotary cutter. This can be attributed to its thin titanium blade, which facilitated easier penetration into the agar gel phantom and reduced resistance during reciprocating motion. As a result, the swing cutter required only 0.02 N of force on average, whereas the rotary cutter, with its 3D-printed blade, needed higher force (0.07 N) to initiate and maintain cutting.

V. DISCUSSION AND CONCLUSION

Compared to the output force reported in [16], our 3-DoF tools can deliver the same level of force, sufficient for operations required in clinical procedures. We used only a single embedded magnet, which significantly reduces system weight, size, and instability due to magnetic interference. Moreover, while traditional 3-DoF robots typically require three individual actuators, our design revolutionizes this by using a force-guided strategy. This approach directly drives



(a) Cutting lengths achieved across trials.



(b) Corresponding cutting forces measured (averaged).

Fig. 5: Cutting performance evaluation of the swing and rotary cutters on 1% agar gel. (a) Left: Experimental setup showing tool placement on agar gel mounted on a force sensor. Right: Example cut lines produced in the agar phantom. (b) The force values represent the average normal force F_z (over the entire cutting duration) recorded during each trial.

the tip through coordinated magnetic torque control, eliminating the need for embedded actuators or tethered power supplies, and making the system highly compact and suitable for constrained surgical environments. The swing and rotary cutters enabled independent pitch, roll, and yaw control for dexterous tissue resection. The rotary cutter provided continuous rotation with precise control, while the swing cutter mimicked sawing motions. Both performed reliably in brain-like agar phantoms, supporting use in procedures like corpus callosotomy and tumor resection. These findings highlight the potential of our 3-DoF magnetic manipulator as a simple yet versatile alternative to cable-driven tools. Future work will focus on in vivo validations, exploring feedback-based control strategies, and extending the magnetic actuation paradigm to enable bimanual coordination. This study marks a significant step toward translating magnetically driven surgical robots into clinical neurosurgical practice.

ACKNOWLEDGMENT

We would like to thank Alex Zhang for his assistance with the 3D printing of cutters.

REFERENCES

[1] C. He, R. Nguyen, H. Mayer, L. Cheng, P. Kang, D. A. Aubeeluck, G. Thiong', E. Fredin, J. Drake, T. Looi, *et al.*, "Magnetically actuated

dexterous tools for minimally invasive operation inside the brain," *Science Robotics*, vol. 10, no. 100, p. eadk4249, 2025.

[2] Y. Kim, E. Genevriere, P. Harker, J. Choe, M. Balicki, R. W. Regenhardt, J. E. Vranic, A. A. Dmytriw, A. B. Patel, and X. Zhao, "Telerobotic neurovascular interventions with magnetic manipulation," *Science Robotics*, vol. 7, no. 65, p. eabg9907, 2022.

[3] G. Pittiglio, F. Leuenberger, M. Mencattelli, M. McCandless, E. O'Leary, and P. E. Dupont, "Magnetic ball chain robots for cardiac arrhythmia treatment," *IEEE Transactions on Medical Robotics and Bionics*, 2024.

[4] S. Ernst, F. Ouyang, C. Linder, K. Hertting, F. Stahl, J. Chun, H. Hachiya, D. Bansch, M. Antz, and K.-H. Kuck, "Initial experience with remote catheter ablation using a novel magnetic navigation system: magnetic remote catheter ablation," *Circulation*, vol. 109, no. 12, pp. 1472–1475, 2004.

[5] Q. Yang, Á. Enríquez, D. Devathasan, C. A. Thompson, D. Nayee, R. Harris, D. Satoski, B. Obeng-Gyasi, A. Lee, R. T. Bentley, *et al.*, "Application of magnetically actuated self-clearing catheter for rapid in situ blood clot clearance in hemorrhagic stroke treatment," *Nature Communications*, vol. 13, no. 1, p. 520, 2022.

[6] Y. Piskarev, J. Shintake, C. Chautems, J. Lussi, Q. Boehler, B. J. Nelson, and D. Floreano, "A variable stiffness magnetic catheter made of a conductive phase-change polymer for minimally invasive surgery," *Advanced Functional Materials*, vol. 32, no. 20, p. 2107662, 2022.

[7] M. Tiryaki, Y. Elmaccioğlu, and M. Sitti, "Magnetic guidewire steering at ultrahigh magnetic fields," *sci adv* 9: eadg643, 2023.

[8] C. Forbrigger, A. Lim, O. Onaizah, S. Salmanipour, T. Looi, J. Drake, and E. D. Diller, "Cable-less, magnetically driven forceps for minimally invasive surgery," *IEEE Robotics and Automation Letters*, vol. 4, no. 2, pp. 1202–1207, 2019.

[9] M. Nica, C. Forbrigger, and E. Diller, "A novel magnetic transmission for powerful miniature surgical robots," *IEEE/ASME Transactions on Mechatronics*, vol. 27, no. 6, pp. 5541–5550, 2022.

[10] O. Onaizah and E. Diller, "Tetherless mobile micro-surgical scissors using magnetic actuation," in *2019 International Conference on Robotics and Automation (ICRA)*. IEEE, 2019, pp. 894–899.

[11] A. Lim, A. Schonewille, C. Forbrigger, T. Looi, J. Drake, and E. Diller, "Design and comparison of magnetically-actuated dexterous forceps instruments for neuroendoscopy," *IEEE Transactions on Biomedical Engineering*, vol. 68, no. 3, pp. 846–856, 2020.

[12] Y. Deng, M. Roshanfar, H. Mayer, C. He, J. Drake, T. Looi, and E. Diller, "Towards bimanual operation of magnetically actuated surgical instruments," in *2024 10th IEEE RAS/EMBS International Conference for Biomedical Robotics and Biomechanics (BioRob)*. IEEE, 2024, pp. 1295–1300.

[13] C. Freschi, V. Ferrari, F. Melfi, M. Ferrari, F. Mosca, and A. Cuschieri, "Technical review of the da vinci surgical telemanipulator," *The International Journal of Medical Robotics and Computer Assisted Surgery*, vol. 9, no. 4, pp. 396–406, 2013.

[14] C. He, R. H. Nguyen, C. Forbrigger, J. Drake, T. Looi, and E. Diller, "A hybrid steerable robot with magnetic wrist for minimally invasive epilepsy surgery," in *2023 IEEE International Conference on Robotics and Automation (ICRA)*. IEEE, 2023, pp. 6830–6836.

[15] Q. Peyron, Q. Boehler, P. Rougeot, P. Roux, B. J. Nelson, N. Andreff, K. Rabenorosoa, and P. Renaud, "Magnetic concentric tube robots: Introduction and analysis," *The International Journal of Robotics Research*, vol. 41, no. 4, pp. 418–440, 2022.

[16] C. Forbrigger, E. Fredin, and E. Diller, "Evaluating the feasibility of magnetic tools for the minimum dynamic requirements of microneurosurgery," in *2023 IEEE International Conference on Robotics and Automation (ICRA)*. IEEE, 2023, pp. 4703–4709.

[17] H. J. Marcus, K. Zareinia, L. S. Gan, F. W. Yang, S. Lama, G.-Z. Yang, and G. R. Sutherland, "Forces exerted during microneurosurgery: a cadaver study," *The International Journal of Medical Robotics and Computer Assisted Surgery*, vol. 10, no. 2, pp. 251–256, 2014.

[18] R. Pomfret, G. Miranpuri, and K. Sillay, "The substitute brain and the potential of the gel model," *Annals of neurosciences*, vol. 20, no. 3, p. 118, 2013.

[19] J. J. Abbott, E. Diller, and A. J. Petruska, "Magnetic methods in robotics," *Annual Review of Control, Robotics, and Autonomous Systems*, vol. 3, no. 1, pp. 57–90, 2020.

[20] A. Schonewille, C. He, C. Forbrigger, N. Wu, J. Drake, T. Looi, and E. Diller, "Electromagnets under the table: an unobtrusive magnetic navigation system for microsurgery," *IEEE Transactions on Medical Robotics and Bionics*, 2024.